The GMT-consortium large earth finder (G-CLEF): an optical echelle spectrograph for the Giant Magellan Telescope (GMT)

Szentgyorgyi, Andrew, Baldwin, Daniel, Barnes, Stuart, Bean, Jacob, Ben-Ami, Sagi, et al.

Andrew Szentgyorgyi, Daniel Baldwin, Stuart Barnes, Jacob Bean, Sagi Ben-Ami, Patricia Brennan, Jamie Budynkiewicz, Daniel Catropa, Moo-Young Chun, Charlie Conroy, Adam Contos, Jeffrey D. Crane, Daniel Durusky, Harland Epps, Ian Evans, Janet Evans, Valery Fishman, Anna Frebel, Thomas Gauron, Dani Guzman, Tyson Hare, Bi-Ho Jang, Jeong-Gyun Jang, Andres Jordan, Jihun Kim, Kang-Min Kim, Yunjong Kim, Sungho Lee, Mercedes Lopez-Morales, Claudia Mendes de Oliveira, Kenneth McCracken, Stuart McMuldroch, Joseph Miller, Mark Mueller, Jae Sok Oh, Cem Onyuksel, Byeong-Gon Park, Chan Park, Sung-Joon Park, Charles Paxson, David Phillips, David Plummer, William Podgorski, Adam Rubin, Andreas Seifahrt, Daniel Stark, Joao Steiner, Alan Uomoto, Ronald Walsworth, Young-Sam Yu, "The GMT-consortium large earth finder (G-CLEF): an optical echelle spectrograph for the Giant Magellan Telescope (GMT)," Proc. SPIE 10702, Ground-based and Airborne Instrumentation for Astronomy VII, 107021R (6 July 2018); doi: 10.1117/12.2313539

SPIE.

Event: SPIE Astronomical Telescopes + Instrumentation, 2018, Austin, Texas, United States

The GMT-Consortium Large Earth Finder (G-CLEF): An optical echelle spectrograph for the Giant Magellan Telescope (GMT)

Andrew Szentgyorgyi*[a], Daniel Baldwin[a], Stuart Barnes[a], Jacob Bean[e], Sagi Ben-Ami[a], Patricia Brennan[a], Jamie Budynkiewicz[a], Daniel Catropa[a], Moo-Yung Chun[g], Charlie Conroy[a], Adam Contos[f], Jeffrey D. Crane[c], Daniel Durusky[a], Harland Epps[i], Ian Evans[a], Janet Evans[a], Valery Fishman[a], Anna Frebel[h], Thomas Gauron[a], Dani Guzman[d], Tyson Hare[c], Bi-Ho Jang[g], Jeong-Gyun Jang[g], Andres Jordan [d], Jihun Kim[g], Kang-Min Kim[g], Yunjong Kim[g], Sungho Lee[g], Mercedes Lopez-Morales[a], Claudia Mendes de Oliveira[j], Kenneth McCracken[a], Stuart McMuldroch[a], Joseph Miller[a], Mark Mueller[a], Jae Sok Oh[g], Cem Onyuksel[a], Byeong-Gon Park[g], Chan Park[g], Sung-Joon Park[g], Charles Paxson[a], David Phillips[a], David Plummer[a], William Podgorski[a], Adam Rubin[k], Andreas Seifahrt[e], Daniel Stark[b], Joao Steiner[j], Alan Uomoto[c], Ronald Walsworth[a] and Young-Sam Yu[g].

[a] Harvard-Smithsonian Center for Astrophysics, 60 Garden St., Cambridge, MA 02140

[b] Steward Observatory, University of Arizona, 933 North Cherry St., Tucson, AZ, 85721

[c]The Observatories of the Carnegie Institution for Science, 813 Santa Barbara St., Pasadena, CA 91101

[d] Pontificia Universidad Catolica de Chile, Vicuna Mackenna 4860, Macul, Santiago, Chile

[e] University of Chicago, 640 S. Ellis Ave, Chicago, IL 60637

[f] Giant Magellan Telescope Organization, 465 Halstead St., Pasadena, CA, 91107

[g] Korean Astronomy and Space Science Institute (KASI) 776, Daedeokdae-ro, Yuseong-gu, Daejeon, Republic of Korea

[h] Massachusetts Institute of Technology, Kavli Institute for Astrophysics and Space Research, 77 Massachusetts Ave., Cambridge, MA 02139

[i]UCO/Lick Observatory, University of California, Santa Cruz, CA 95064

[j]Universidade de São Paulo, Rua do Matão 1226, 05508-900, São Paulo, Brazil

[k]Department of Particle Physics and Astrophysics, Weizmann Institute of Science, 234 Herzl St.., Rehovot, Israel

ABSTRACT

The GMT-Consortium Large Earth Finder (G-CLEF) is an instrument that is being designed to exceed the state-of-the-art radial velocity (RV) precision achievable with the current generation of stellar velocimeters. It is simultaneously being designed to enable a wide range of scientific programs, prominently by operating to blue wavelengths (> 3500Å). G-CLEF will be the first light facility instrument on the Giant Magellan Telescope (GMT) when the GMT is commissioned in 2023. G-CLEF is a fiber-fed, vacuum-enclosed spectrograph with an asymmetric white pupil echelle design. We discuss several innovative structural, optical and control system features that differentiate G-CLEF from previous precision RV instruments.

Keywords: Optical spectroscopy, echelle spectrographs, extremely large telescopes, exoplanets, precision radial velocity, stellar astrophysics.

* saint@cfa.harvard.edu; Phone: 1-617-495-7379

Ground-based and Airborne Instrumentation for Astronomy VII, edited by Christopher J. Evans, Luc Simard, Hideki Takami, Proc. of SPIE Vol. 10702, 107021R · © 2018 SPIE · CCC code: 0277-786X/18/$18 · doi: 10.1117/12.2313539

1. INTRODUCTION

The GMT-Consortium Large Earth Finder (G-CLEF) is the first major scientific instrument that will be delivered to the Giant Magellan Telescope (GMT)[1] at first light. Since the design, characteristics and capabilities have been described in earlier publications[2][3][4]as well as other publications in these proceedings[5][6][7][8][9][10], the subject matter is confined to new technical developments and aspects of the G–CLEF design that have not been published previously.

There has been a surprising evolution of the science case for G-CLEF. As originally conceived in 2008, G-CLEF was primarily a instrument for precise radial velocity (PRV) measurements of stars, so as to measure the mass of exoplanets orbiting those stars. The goal for G-CLEF was to detect an Earth-twin exoplanet orbiting a Solar-like star in the habitable zone, where the surface temperature is compatible with the presence of water in liquid phase. This requires a precision of 10 cm/sec achieved with repeated measurements. The current "record" for smallest reflex motion measurement is that of HD20794[11] – a value of 56 cm/sec in 187 data points – a V_{Mag} = 4.26 star observed with the HARPS spectrograph, deployed at the la Silla 3.5m telescope.

After extensive trade studies, it was determine that G-CLEF would be fiber-fed and deployed at the gravity-invariant station of the GMT (see, Figure 1). Situating G-CLEF so close to the telescope in the dome, rather than a more remote location that did not move with the telescope has presented some significant engineering challenges, especially in the area of thermal control and vibration isolation. The thermal stability of G-CLEF is of paramount importance to achieve PRV goals, so the spectrograph has to be exquisitely thermally controlled. However, the outer envelope of G-CLEF must be maintained in thermal equilibrium with the telescope chamber to avoid the creation of thermal plumes and turbulence that would affect dome seeing. Nonetheless, this choice allowed the shortest fiber run of any PRV–capable instrument (17 m). Low fiber throughput at the blue end of the of the visible spectrum is debilitating to fiber fed instruments with longer fiber runs. The efficiency of most fiber–fed instruments becomes vanishingly low at ~3900Å–4000Å or bluer. G-CLEF will have good efficiency to 3500Å which broadens the passband for PRV observations, but also opens up a discovery space measuring chemical abundances in extremely metal poor star populations.

Most PRV spectrographs are wavelength calibrated with hollow cathode thorium-argon (ThAr) lamps. In the last decade, there has been a revolution in the development of alternative calibrators, especially laser frequency combs[12][13][14], passive etalons[15][16] and actively stabilized etalons[17][18]. This activity has been stimulated by several factors, primarily the choice of industry to halt production of metal cathode ThAr lamps. The alternative – thorium oxide cathode lamps – produce contaminated spectra that degrade RV precision. While ThAr lamps have been the "gold standard" for RV calibration, this choice has carried a penalty that limits the discovery space of instruments calibrated with ThAr lamps. The argon that is used to excite thorium produce high intensity features in the red that are useless for calibration but cause crippling scattered light in a spectrograph. It is necessary to limit the passband of ThAr-calibrated PRV instruments to wavelengths shortward of ~6800Å. The traditional alternative to ThAr lamps as wavelength calibrators for high dispersion spectrographs are iodine (I_2) absorption cells, however these have an even more restrictive passband (~5000–6000Å).

By adopting new calibrators, we extend the operating passband to 9000Å (Goal:9500Å). This increases the utility of G–CLEF for low–mass star science, especially the search for Earth–twins orbiting M-type stars. The cosmological reach of G-CLEF is also extended. Lyman α is red shifted to 6800Å at a z of 4.6, whilst at 9000Å it is redshifted to a z of 6.4, and z = 6.8 red shifts it to 9500Å. The extended red response of G-CLEF will enable observations of the era of structure formation in the early Universe.

The recent launch of the TESS[19] satellite will provide a rich catalogue of bright, nearby exoplanets for G-CLEF to observe, especially to search for biomarkers in exoplanet atmospheres. It has only been recognized lately, since G-CLEF was first conceived, that a particularly useful spectral feature will be the diatomic oxygen (O_2) A-band feature near 7600Å[20][21]. The disequilibrium balance of molecular oxygen in the Earth's atmosphere is entirely due to biological activity. The efficiency of G-CLEF in this spectral region is quite high, so G-CLEF will be a powerful tool to search for life beyond the Solar System.

Interpretation of the kilonova afterglow of the recent LIGO/Virgo detection of a merging neutron star binary, the first gravity–wave event localized and detected in the optical band, rests on our understanding of heavy r-process nucleosynthesis[22]. Observed r-process element signatures in the oldest, most metal-poor stars provide the best empirical data to study the astrophysical sites of the r-process, especially when found in dwarf galaxies (e.g. Reticulum II[23]). R-process stars can also be age dated, which makes them particularly important for near-field cosmology and our understanding of early galaxy formation. Measurements of the radioactive elements thorium, and, especially, uranium, are

needed, but require high–resolution (R>50,000) spectra measured with very high signal–to–noise (S/N~500) to yield precise ages. Currently, only stars with V<12 are observable with existing facilities[24], but G-CLEF could access much fainter candidates. Example exposure times would be 4h for V=14, 12h for V=15. A sample of ~30-50 objects would conclusively map out the ages of the most metal-poor stars. Faint (V>18) dwarf galaxy stars could also be accessed to aid identification of future r-process galaxies and determining the neutron star merger rate from the population of dwarf galaxies. It is to be noted that the only detected line of uranium, a critical nucleo–chronometer, in a stellar spectra is a feature at 3859Å, again underscoring the importance of G-CLEF's good throughput in the deep blue.

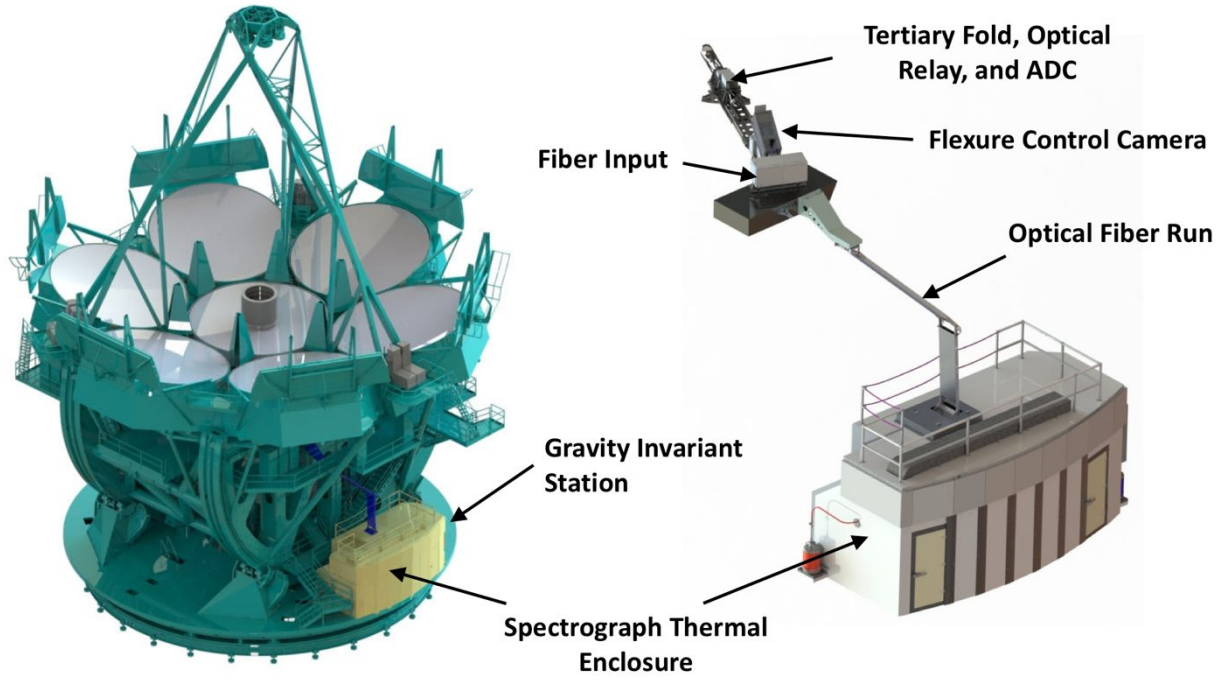

Figure 1: *Left Panel*–G_CLEF as mounted on the GMT. *Right panel*–Blow–up of the external view of the G–CLEF telescope interface, the fiber run and the spectrograph thermal enclosure.

G-CLEF operates in several stand–alone modes and also in concert with several other instruments that are being developed for the GMT. In stand alone-mode, there are four distinct observing modes enabled by four different fiber runs. They are:

- High Throughput (HT) mode – A mode which is to be used when the greatest throughput is desired. High throughput is achieved at the expense of resolution.
- Medium Resolution (MR) Mode – A mode tuned to the resolution requirements of stellar abundance investigations while simultaneously maximizing throughput.
- Precision Radial Velocity (PRV) Mode – A mode optimized for PRV measurements, with mode scrambling.
- Non-Scrambled PRV (NS-PRV) Mode – High resolution mode that has enhanced throughput compared the PRV mode, achieved by eliminating mode scrambling.

The characteristics of these modes are summarized in Table 1.

In addition to the stand–alone modes, G–CLEF can be operated with several other instruments. The Australian GMT consortium members are contributing a fiber positioner for multi–object spectroscopy (MOS) – the Many Instrument Fiber System (MANIFEST) – which will provide a multiplex of 40 at a resolution of 35,000[25] when operated with G-CLEF. It was only recently realized that when the GMT Near InfraRed Spectrograph (GMTNIRS[26]) operated in natural guide star adaptive optics (AO) mode – as opposed to laser guide star AO – the optical wavelength light entering GMTNIRS could be shunted to G-CLEF with an optical beam splitter. This fiber would enable simultaneous G-CLEF/GMTNIRS observations in a total passband of 3500Å to 5.3μ at a resolution of 85,000, with a small dropout between 9500Å and 1.15μ.

G-CLEF is also including a "spare" focal station to potentially feed other instruments in the future.

Table 1: Properties of the G-CLEF stand-alone modes. The GMT beam is f/8, but converted to f/3 at the fiber input to minimize focal ratio degaradation. It is converted back to f/8 at the G-CLEF fiber slit in the sprectrograph. For PRV and NS-PRV modes, the telescope pupil is sliced into seven subapertures conjugated to the facets of the primary itself (see Figure 1).

Mode	f/8 Slit Dia. (arcsec)	f/8 Slit Dia. (μm)	Res.	Comments
HT	1.2	1200	19,000	Round optical fiber
MR	0.8	800	35,000	Round optical fiber
PRV	0.8	267	105,000	Octagonal optical fiber, pupil sliced, scrambled
NS-PRV	0.8	267	105,000	Octagonal optical fiber, pupil sliced, not scrambled

A system – level diagram of the flow of light within G-CLEF is shown in Figure 2. The GMT has a instrument–rotating platform – the Gregorian Instrument Rotator (GIR) – which is supported on the Instrument Platform (IP) – see Figure 3. Most folded–port instruments are mounted on the GIR. The G-CLEF telescope interface, the G–CLEF Front End Assembly (GCFEA), is split between the GIR and IP. The GIR segment (GCGIR) consists of the tertiary fold mirror, an alignment/focusing target wheel and a refractive triplet collimator. The GCGIR is deployable, i.e. it is inserted into the telescope beam for G-CLEF observations and retracted when other instruments are in use. The IP segment (GCIP) houses the atmospheric dispersion compensator (ADC), a focusing triplet, calibration light injectors and the stand–alone fiber mode selector. "Science" light – both the science target and sky subtraction light are conveyed from the GCIP to the spectrograph by the science fibers (GCSFIB). MANIFEST and GMTNIRS interface directly to the spectrograph. Calibration light is routed from the calibration light system (GCCLS) to the input of GCSFIB by the calibration fibers (GCCFIB). Several state–of–the–art light sources are too large to fit in the GCCLS, so they will be mounted externally and interfaced to the GCCLS with integrating spheres internal to the GCCLS.

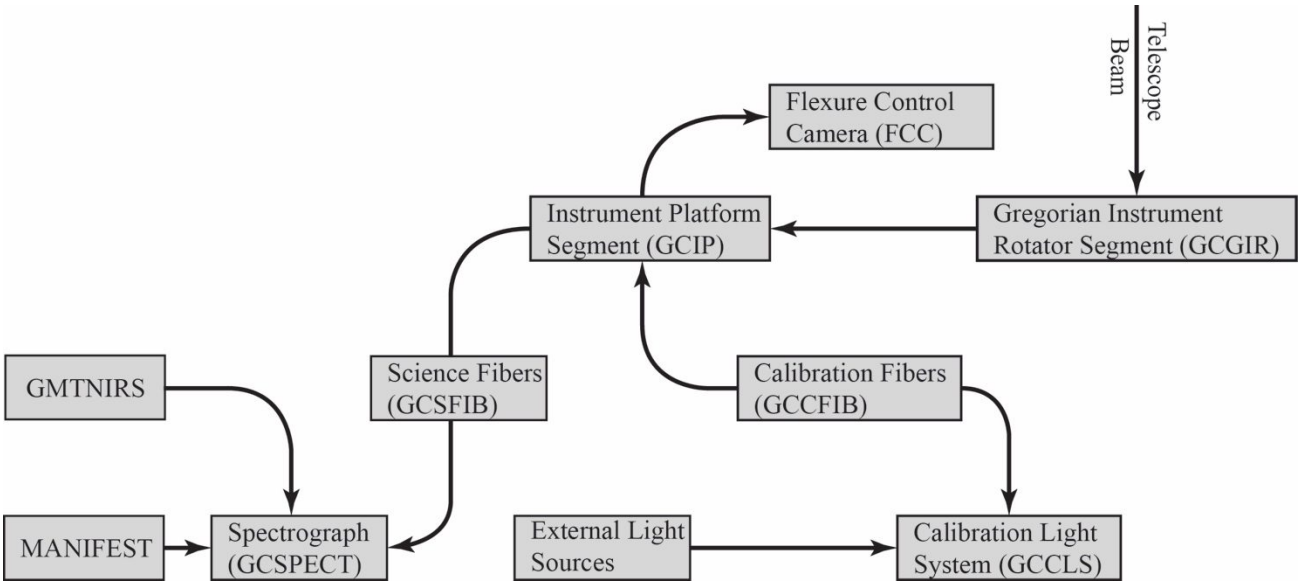

Figure 2: The flow of light within G-CLEF

The physical arrangement of the "front end" assembly – the GCFEA is shown in Figure 3 – i.e. the aggregate of the FCC, GCIP and GCGIR. The requirement to minimize the science fiber length for good blue wavelength throughput has led to the design that is split between the IP and GIR. An additional consideration was the need for a dedicated tertiary mirror. The GMT has a facility tertiary fold mirror, however it is utilized exclusively for infrared instrumentation, so the reflective coating on the facility tertiary is incompatible with the G-CLEF passband. As a result, G-CLEF has a dedicated tertiary. The GIR is fixed during G-CLEF observations, so the G-CLEF field is not derotated.

In this paper we first give a brief description of the optomechanics, with an emphasis on innovations that have been developed since the last published report on G-CLEF[2]. We then discuss the thermomechanical issues that bear on building a PRV instrument that is expected to outperform the current generation of PRV spectrographs. Given the unique character of the GMT control system, the requirements for focus and guide at the instrument focal plane are different from most other instruments. We discuss these under the rubric of a "flexure control camera". We discuss the strategy for calibration G-CLEF and conclude with a project status. G-CLEF stands at the threshold of its critical design review, scheduled to occur shortly after the end of this SPIE conference.

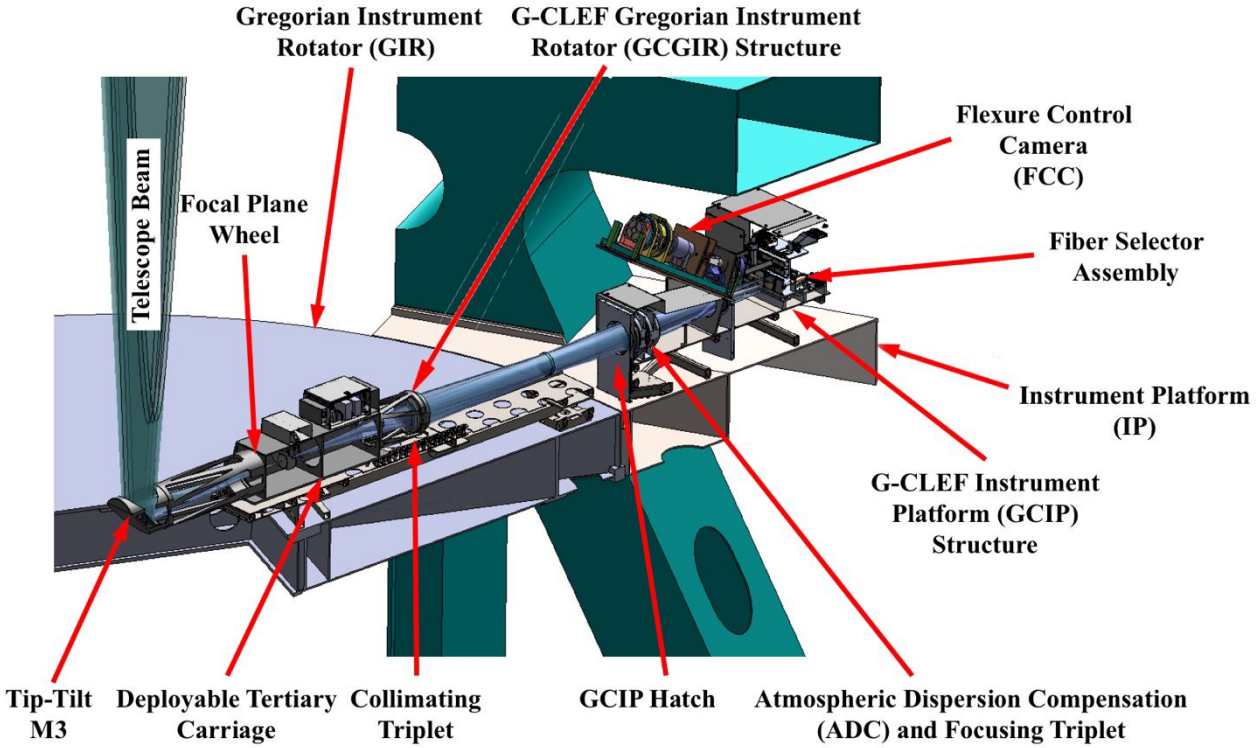

Figure 3: The G-CLEF telescope interface or "front end" – GCFEA. This is split into three functional units – the GCGIR which is mounted on the GMT Gregorian instrument rotator. The GCIP, which is mounted on the static instrument platform and the FFC, which is mounted on the GCIP.

2. OPTICAL INNOVATIONS

In this section, after a brief context–setting description of G-CLEF optomechanics is provided, we discuss the evolution of and innovations in the G–CLEF design. More background information on the these innovations appears elsewhere in these proceedings[7]. The optical design is discussed in detail elsewhere previous proceedings[8].

The first order parameters of the G-CLEF spectrograph design are presented in Table 2. The optical train within the spectrograph and the major optomechanical subsystems are illustrated in Figure 4. The prominent feature of the design is the adoption of an asymmetric, white pupil design, where the resolution is set by the initial spectrograph beam diameter (300 mm), which impinges on the echelle grating. The beam is then reduced to 200 mm by the pupil transfer mirror (M2) to make it possible to use comparatively smaller lenses in the cameras. The creation of a pupil at the camera entrance aperture has the added benefit of minimizing color–dependent aberrations. The spectrograph is quasi–Littrow – a small "γ angle" pitch to the echelle grating is introduced to separate the beams within the spectrograph optical train and thus to make the spectrograph buildable. The near–Littrow geometry choice minimizes anamorphism.

Table 2: Summary of G-CLEF spectrograph parameters. We have adopted a "baseline" pixel size of 9 μ, which will ultimately depend on which vendor is chosen to supply the spectrograph focal plane.

G-CLEF Property	Value	G-CLEF Property	Value
Spectrograph Beam Diameter	300 mm	Spectrograph Focal Ratio	F/8
Design Paradigm	Asymmetric white pupil	Spectrograph Geometry	Quasi-Littrow
Echelle Grating Facet Count	3	Collimator focal length	2400 mm
Fiber Output Focal Ratio	F/3	Pupil Xfer focal length	1600 mm
Camera Beam Diameter	200 mm	Pup.Xfer Mirr./Cam. Reduction	450/1600 = 0.2813
Camera Focal Ratio	F/2.25	PRV Slit Image Size	0.075 mm
Camera Focal Length	450 mm	Baseline Pixel Size	0.010 mm
Passband	3500Å-5400Å & 5400Å-9500Å	Camera lens count (blue/red)	8/7
Exposure Meter?	Yes	Field Flattener?	Yes

The passband is quite broad, so it is divided into two smaller passbands, which makes the optical design of the camera more tractable. The camera designs consist mostly of spherical surfaces – each camera has a single aspheric surface. A feature of white pupil designs is a cylindrical field curvature that requires correction. This has been typically corrected with a toroidal field flattener. However, since this lens must be located some distance in front of the focal plane, correction is not optimal. The G-CLEF design accomplishes this correction with a cylindrical Mangin mirror at the internal focus of the spectrograph[27]. However the Mangin mirror must be wedged and tilted to mitigate a potentially crippling ghost produced by a parallel geometry Mangin mirror[7].

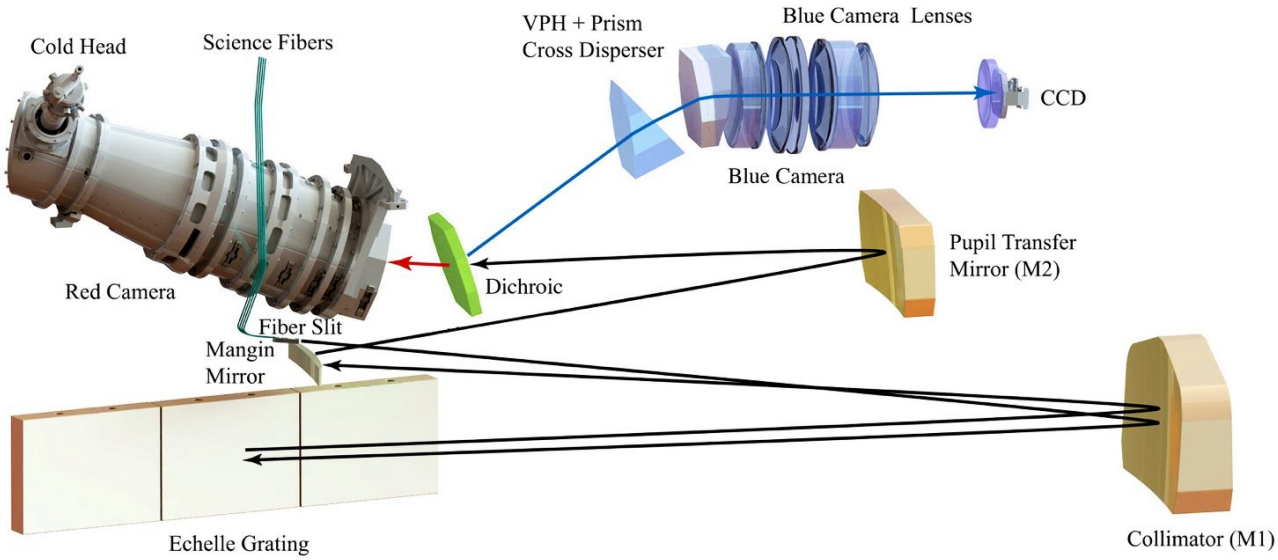

Figure 4: The path of the optical beam within the G-CLEF spectrograph.

In order to achieve radial velocity precision in observations of Solar–analogue stars at and below the 1 m/s level, spectrographs must have resolutions greater than 100,000. The resolution of a spectrograph scales as the ratio of the diameter of the spectrograph beam to the telescope aperture ($R \propto \Phi_{Spect}/\Phi_{Tel}$). For this reason, the 25.4 m aperture of the GMT must be sliced into 7 subapertures to permit a physically realizable spectrograph design where $R > 100{,}000$ and $\Phi_{Spect} \leq 300\ mm$. The GMT pupil is ideally suited to lossless pupil slicing and is accomplished with the optical designs shown in Figure 5. However, this does introduce a complication that in PRV and NS–PRV modes the stellar image must be aligned with the aperture in the fiber mirror at the focus of the GCFEA relay system, and the telescope pupil image

needs to be aligned with the pupil slicer. These simultaneous alignments can be achieved with the two degrees of freedom provided by the pointing of the telescope and the tip–tilt tertiary mirror. Nonetheless, the pupil alignment needs to be established at the start of each new pointing and possibly checked at the beginning of each observation. For this purpose, a deployable pupil viewer is included in the PRV and NS-PRV optical trains to align the pupil.

Another issue that has been addressed in the G-CLEF spectrograph design is that of field flattening, in the sense of measuring spatially dependent sensitivity variations in the CCD response. It is desirable to be able to field–flatten the focal plane of the spectrograph, especially to measure pixel–to–pixel sensitivity variations. Sensitivity will depend on several factors. The properties of the detector medium itself, how uniformly it is pixelated, and the illumination geometry itself all effect individual pixel sensitivity. The illumination of any given pixel is very monochromatic in an echelle spectrograph, so the properties of the anti-reflection (AR) coating is also a critical factor in pixel sensitivity. For this reason it is essential that flat field illumination must mimic the wavelength distribution of science illumination. It is also essential that the regions within the inter–order nulls of the echellogram be illuminated adequately by the field–flattening light source to measure pixel–to–pixel sensitivity variations. In cross–dispersed, slit–fed echelle spectrograph this is accomplished relatively straightforwardly by illuminating a over-long slit that fills the nulls between the orders. While this might be solved by introducing additional, over–sized optical fibers at the spectrograph pseudo–slit that can be back–illuminated, the fibers we would require for G-CLEF are too large to be manufactured. We have developed a novel design that uses an engineered diffuser that converts a beam into an f//8 beam and simulates an oversized fiber slit image. For further details see Ben–Ami et al. in these proceedings[7].

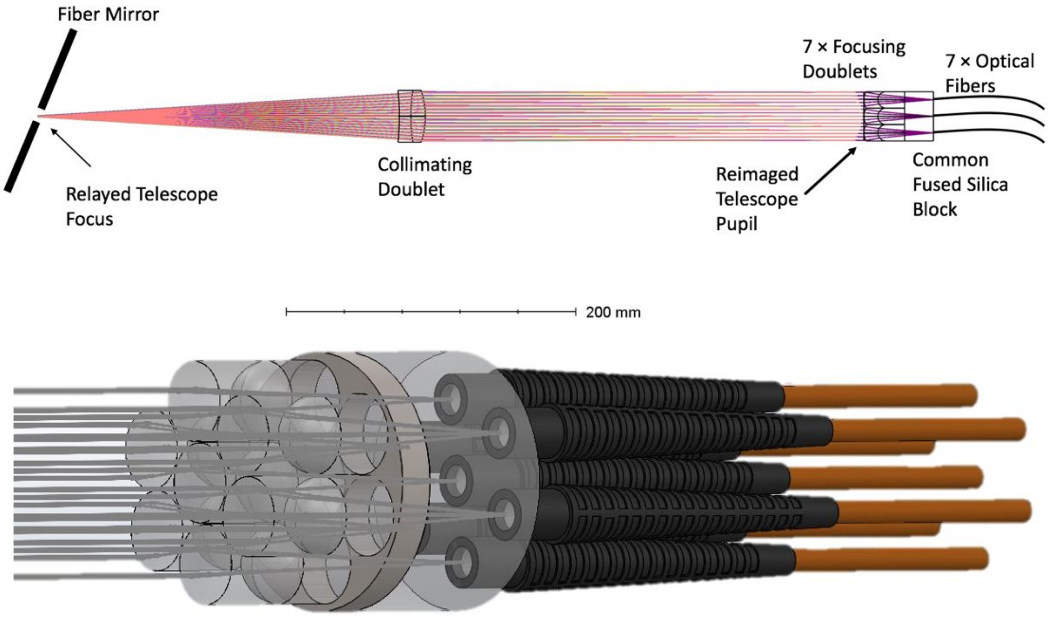

Figure 5: Pupil slicing optics for the PRV and NS-PRV modes

Another innovation we have incorporated into the G–CLEF design is a Bragg–condition cross disperser consisting of a predisperser and a volume phase holographic (VPH) grism. The geometry of this cross–disperser is shown in Figure 6, and is compared with a more traditional VPH grism cross–disperser in the plot appearing in Figure 7.

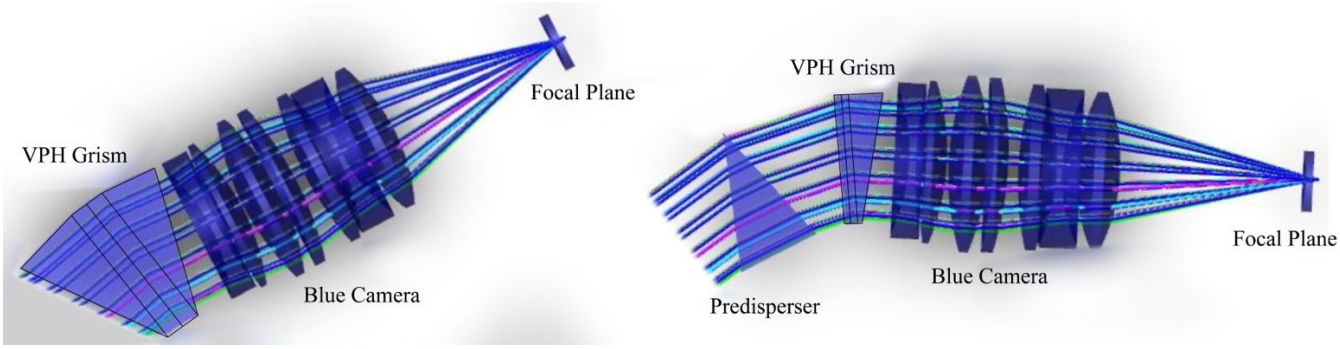

Figure 6: *Left panel*–Standard VPH grism configuration for echelle spectrograph cross dispersion. *Right panel*–Bragg–condition VPH cross disperser used in G–CLEF.

Separating the front prism from the VPH and back prism in the Bragg–condition cross disperser makes it possible to more closely meet the Bragg–condition of the VPH, especially at the blue end of the blue camera passband. This does add an extra air–glass interface to the blue camera optical train, however the net effect is to boost efficiency when compared with a cemented grism. A study of the red camera cross disperser revealed that a similar enhancement is not obtainable there. The red camera has a simple VPH cross disperser. A grism is not necessary. See Ben-Ami in these proceeding for further details[7].

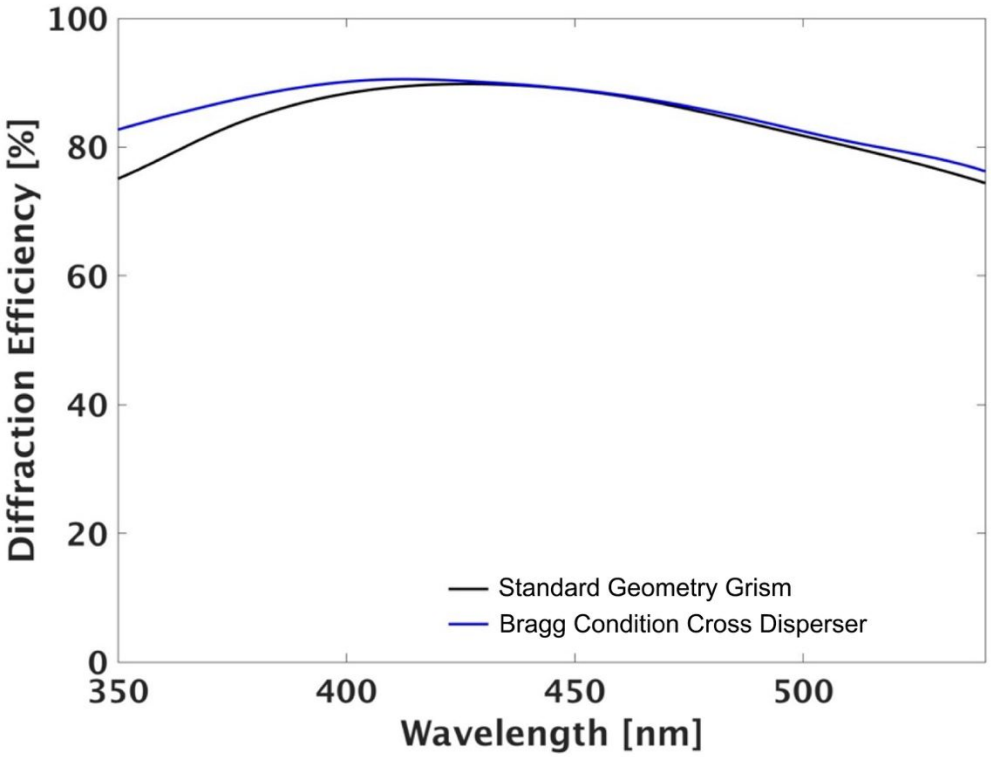

Figure 7:A comparison of the performance of the "standard" grism and Bragg–condition cross dispersers in the blue camera of G-CLEF.

3. THERMOMECHANICAL DESIGN INNOVATION

In the area of thermomechanical design, many of the features of that design have been discussed in earlier publications[28] and publications elsewhere in these proceedings[5][6]. The paramount design drivers for G-CLEF, overall, have been extreme wavelength scale stability for exoplanet mass measurements, a short fiber run to maximize sensitivity in the blue for stellar astrophysics and good red response and high resolution in the red for cosmological investigations the search for biomarkers.

At a fairly early phase in the program, the G–CLEF made a trade study that indicated that a carbon fiber reinforced polymer (CFRP) optical bench provided considerable technical advantage over Invar or mild steel optical benches, from the perspective of maximizing RV precision. These advantages outweighed the added risk and cost of a composite bench when compared with a bench made out of steel or expansion metal. The in-plane coefficient of thermal expansion (CTE) of CFRP is approximately a factor of ten lower than Invar 36, the lowest CTE Invar alloy and at least a factor 100 time lower than mild steel. This translates in vastly reduced thermally induced flexure and enhanced wavelength scale stability.

The in–plane modulus of CFRP is only moderately lower than Invar (100 GPa vs. 140 GPa) but the density is of CFRP is 5.3 times lower than Invar 36. As a result, there is a significant advantage in the stiffness–to–mass ratio, resulting is a considerably lighter structure of comparable stiffness. As the design of the GMT itself has progressed in parallel with the G–CLEF design, it has become apparent that the weight of an Invar 36 based G-CLEF optical bench design would prove problematic for the telescope design team to accommodate.

A final consideration is that the thermal conductivity of Invar is quite low, while the in–plane conductivity of CFRP can be quite high. Thermal gradients within the bench structure that might make it flex are hard to maintain in CFRP. The out–of–plane properties do not compare as favorably with Invar 36, but they are not an issue if the optical bench is designed so that in-plane properties determine the overall CTE, stiffness and thermal conductivity of the bench.

We have developed a number of performance metrics and error budgets that have been described in an earlier publication[29]. A particularly important error budget is the PRV error budget, which is used to track and allocate contributors to RV measurement errors. The metric used when assessing the impact of thermal, structural and dynamic effects on the spectrograph itself is image motion at the detector (IMAD) in the dispersion direction. A trade study between steel, Invar and CFRP revealed that an CFRP meets the PRV error budget allocations for various thermal disturbances, but in general Invar 36 violates our error budget (see Table 3).

Table 3: A comparison of IMAD resulting from a thermal soak and orthogonal gradients as well as root-sum-square (RSS) of all effects for an CFRP and Invar G-CLEF optical bench designs. We have not included entries for mild steel, which are all considerably worse than Invar.

Case	Temp.Change	PRV Budget IMAD (Å,	CFRP IMAD (Å)	CFRP % Budget	Invar IMAD (Å)	Invar % Budget
Soak	+0.001°C	5.4	1.98	37%	0.68	13%
Vertical Gradient	±0.0005°Ç	3.2	1.82	57%	4.18	131%
Lateral Gradient	±0.0005°C	7.8	5.26	67%	64.4	826%
RSS	n/a	10	5.91	59%	64.5	645%

The “egg-crate” structure we have chosen for the optical bench structure is shown in Figure 8. The structure consists of planar elements joined with epoxy–bonded Invar 36 brackets. The extensive properties of the bench are determined almost entirely by the in-plane parameters of CFRP. There is some erosion of overall CTE and conductivity when compared to a pure CFRP structure due to the Invar 36 brackets and epoxy joints. These effect have been include in Table 3. An all-CFRP structure would have better performance, but would drive up the cost of the optical bench. In the coming months,

the G-CLEF design team will collaborate with a composite structure industrial vendor to optimize the bench design and develop a more realistic structural–thermal–optical– performance (STOP) model of G-CLEF.

A final issue concerning composite precision structures is the release of contaminants and water. G-CLEF is vacuum–enclosed. Water and volatiles in the CFRP will outgas under vacuum. Contaminants could coat the optics, thus reducing spectrograph throughput. The release of water will shrink the optical bench secularly. This shrinkage will cause motion of the echellogram on the science detectors. We have worked with a specialist in space system contamination to develop detailed, quantitative models of the expected level of contamination deposits under different fabrications and assembly scenarios. We then used these to develop procedures to mitigate potential contaminants, primarily with an extended vacuum bakeout before the optical bench is delivered to the project. This will also drive out water, but the structure will inevitably be exposed to ambient humidity during spectrograph assembly and alignment. Our consultant has offered guidance on how to minimize re-hydration.

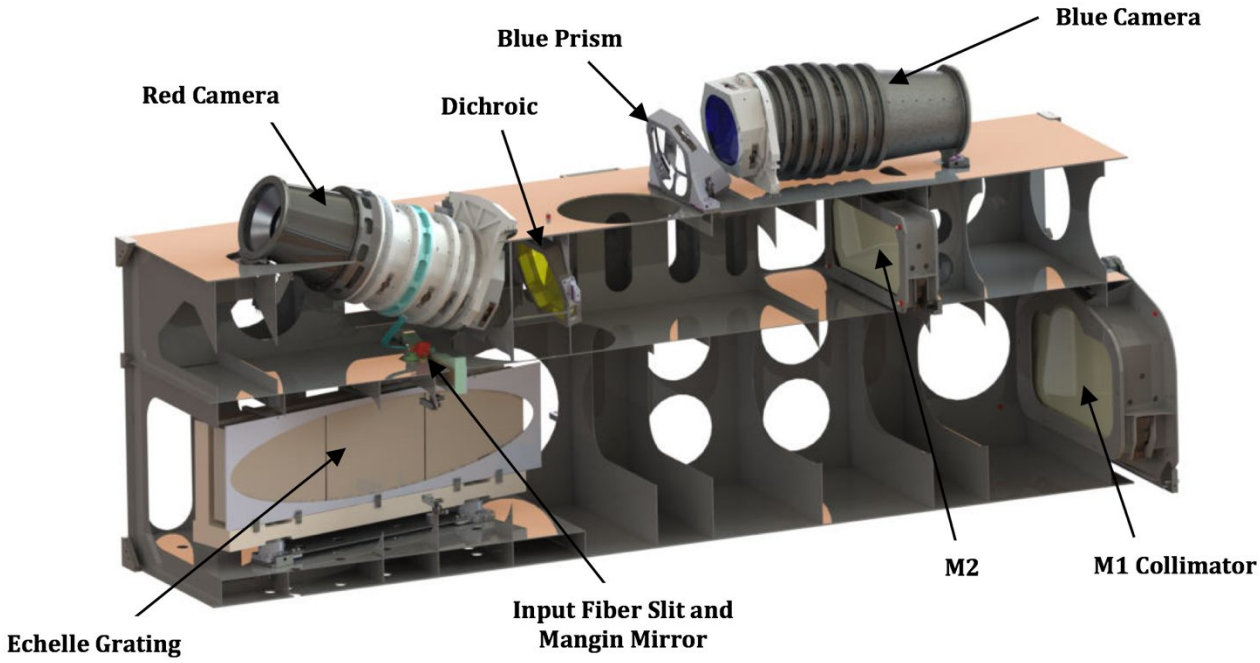

Figure 8: The G-CLEF optical bench with the major spectrograph optical subsystems. The science cryostats for the red and blue cameras are not shown for clarity.

The camera lenses are mounted in stacking bezels shown in Figure 9. All but the last lens in each science camera are bonded into individual Invar bezels, The bezels are radially co–aligned with precision bores. The lenses are mounted to the bezels with two-sided tangential flexures. Many lenses are mounted kinematically, but some lenses require overdetermined structures to meet expected shipping load levels. Stray light baffling is integral to the camera mounts. The cross–dispersers are kinematically mounted and attached to the front of the lens barrels. The structural performance parameters are driven by shipping load resulting from 5G accelerations in a 5°C to 25° temperature range. Operational, survival and earthquake accelerations considerably are lower, over a –5°C to 30°C temperature range.

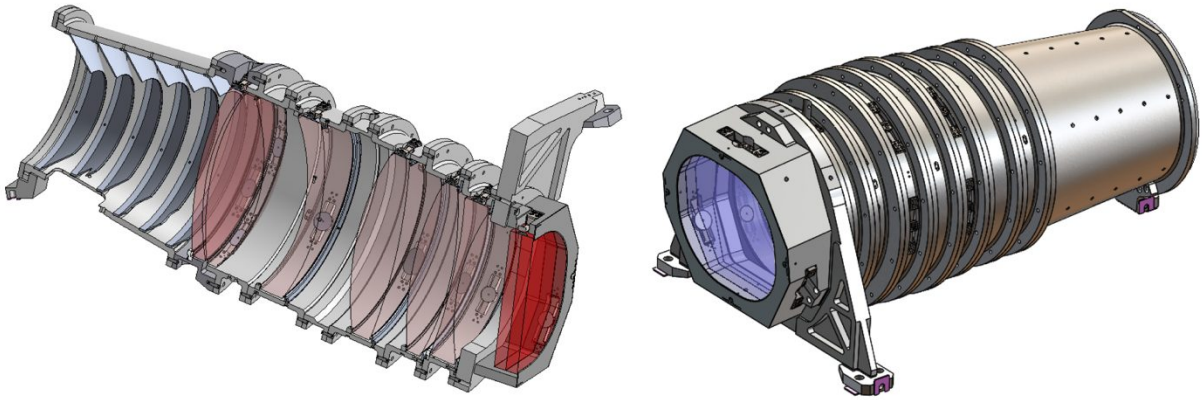

Figure 9: *Left Panel* – Red spectrograph camera and VPH cross disperser, *Right Panel* – Blue spectrograph camera and VPH grism cross disperser.

The spectrograph is vacuum–enclosed, however the science detectors must be operable when the spectrograph is not at vacuum. For this reason, the detector and cold heads have their own vacuum systems, which attach to the back of the camera barrels. The each detector cryostat is sealed with a field flattening lens (see Figure 10). This situation presents an engineering challenge. The field flattener must be able seal against a pressurized spectrograph volume when the cryostat is under vacuum. In the event of catastrophic loss of vacuum in the cryostat, the field flattener must seal again a pressurized cryostat if the spectrograph chamber is evacuated. Finally, it must be positioned at the correct axial station to perform optically, irrespective of the vacuum state of the spectrograph chamber. These requirements have been met with a preloaded design using two O-rings. When the spectrograph is operated in at air, a spacer is needed to slightly re–space the camera optics with respect to the focal plane. This spacer can compensate the axial shift of the field flattener compared with its position under science operating conditions when the spectrograph and cryostat are both at vacuum.

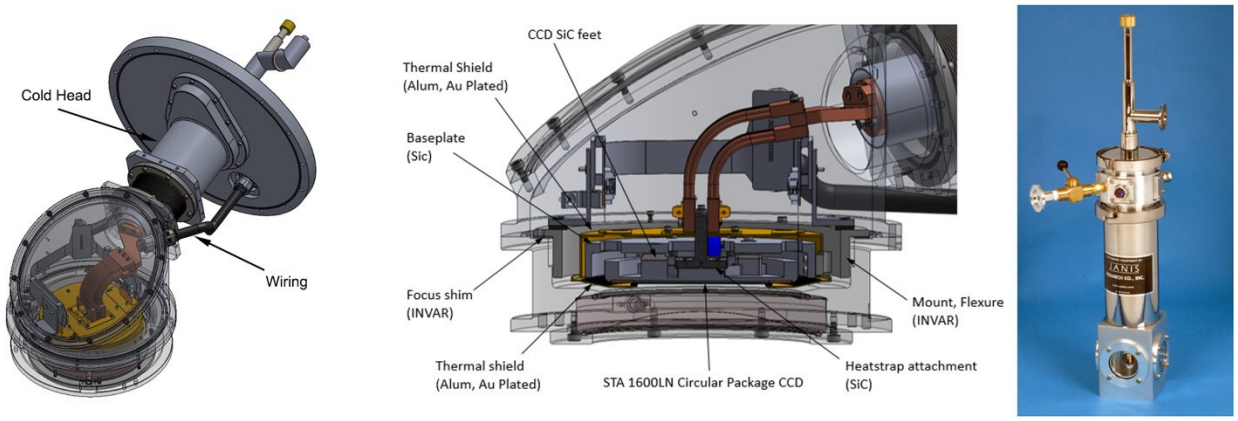

Figure 10: *Left Panel* – Science camera cryostat, *Center Panel* – Detector head, *Right Panel* –Janis SuperTran Continuous Flow Cold Head.

Thermal control of the science imaging arrays is an important consideration for the PRV science we aspire to enable, which hinges on a cryosystem that is thermally stable and vibration free. Our preliminary search included design developed at other observatories, but were proprietary. We also explored the use of mechanical coolers, which posed significant vibration or heat rejection challenges. After a fairly extended canvass of a wide range of possibilities, we discovered that the Janis SuperTran continuous flow cold head met our requirements with an off–the–shelf, commercial product. We have prototyped the G–CLEF focal plane and find that the Janis cold head will offer CCD thermal stability at the few milli–Kelvin level. The driving issue then is the difference between thermal load when the CCD is integrating and when it is being read out. In addition to changing the net thermal dissipation between these two states, the spatial distribution of thermal dissipation also changes. In the case of the STA1600LN CCD, in integrating mode, the dissipation is primarily in

the sense nodes, which dissipate 800 milliwatts at all times. Quiescent dissipation in the serial and parallel registers is zero. Once readout starts, the serial registers dissipate 14/275 milliwatt of power and the parallel registers dissipate 24/105 milliwatts when clocked at 100 kHz/1 MHz. To equilibrate the thermal dissipation between integration and readout the serial registers can be run continuously. We are exploring the possibility of dithering the parallel registers at all time, toggling the charge back and forth by one pixel. This will be well below the dimensions of even the smallest (PRV and NS–PRV) resolution elements. Detailed thermal modeling has indicated that even without this dithering scheme, the PRV error contribution due to differential parallel register thermal dissipation between read–out and integration is ¼ of that we carry in the the PRV error budget.

4. FLEXURE CONTROL SYSTEM

The GMT itself is guided precisely by the Acquisition, Guiding and Wavefront Sensing System (AGWS), which is reviewed by McLeod elsewhere in these proceedings[30]. The AGWS will focus, point and guide the GMT with 1 arcsec absolute accuracy over the GMT's entire observing range, i.e. zenith distance 0° to 60° at all azimuths. For this reason, G–CLEF does not need to have a classical guide function. However, the optical paths of the AGWS and G–CLEF are not common mode, so there will be differential thermal expansion and structural flexure along these two optical paths that needs to be measured and compensated. The Flexure Control Camera measures science target centration on the fiber slit mirror and focus. Error signals are sent to the GMT and the G–CLEF tertiary tip–tilt system to correct pointing and focus. A detailed discussion of the FCC is presented by Oh et al. in these proceedings[9].

The optical design of the FCC is shown in Figure 11. A triplet collimater forms a pupil image that is used for focal measurement and is also the location of neutral density (ND) filters used to extend the dynamic range of the FCC. A four–lens reimager then focuses the guide field on the focal plane of an imaging array. The unvignetted, circular field of view is 90 arcsec, with some vignetting at the corners of the square focal plane detector.

The dynamic range of the FCC is to guide and focus on V ~ 6th to 25th magnitude objects with a control loop that is a maximum of 30 seconds in duration. The FCC will "guide" in two modes. For brighter science objects, guide will be servoed to the light from the science target itself that overflow the aperture in the fiber slit mirror at focus of the GCFEA relay optics. When seeing is superb and there is no overflow or for fainter objects, the FCC will offset guide on objects in the field with the science target. Focus can be monitored with Hartmann masks or a tent prism.

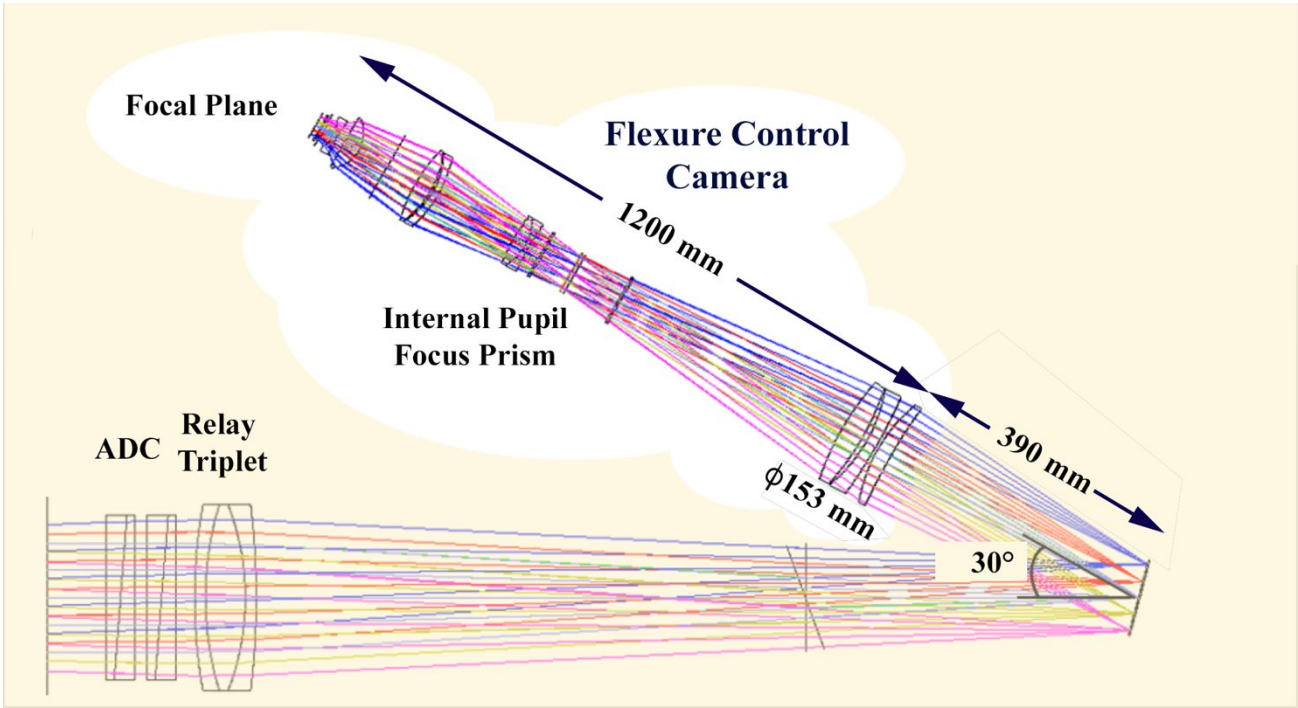

Figure 11: The optical layout of the G-CLEF Flexure Control Camera

The mechanical design of the major components is shown in Figure 12. The optical bench is mounted athermally to an interface plate that attaches to the GCIP. The FCC is divided into four subsystems: the collimator, the focus/filter wheel box, the reimager and the detector module. The focus/filter wheel subsystem consists of two 6–position wheels that are driven by Geneva mechanisms. One wheel contains five ND filters and an open position. The other wheel contains four Hartmann masks, a tent prism and an open position. These are all used to measure focus. The detector module will consist of a commercial, off–the–shelf CCD camera. The camera is mounted on a linear actuator for focus control of the FCC and is derotated.

5. CALIBRATION STRATEGY

Until recently, optical band spectroscopy in general and PRV measurements in particular faced two vexing issues as regards calibration: good blue continuum calibrators and accurate wavelength calibrators. The former problem derived from the fact that even the hottest filaments of incandescent bulbs, operating at ~3200K, have weak output below ~4500Å. Alternative continuum sources, e.g. deuterium lamps have extremely structured spectral energy distribution (SED) longward of 4000Å, and are only useful when used in hybrid light sources with incandescent lamps and band pass filters. The commercial availability of laser driven light sources (LDLS) and supercontinuum lasers has solved this problem. These light sources have relatively smooth spectral energy distributions that extend well below the atmospheric limit of ground based astronomy (~3000Å). The Energetiq LDLS operates in a band extending from 1700Å to 2.1μ and have extremely flat SEDs.

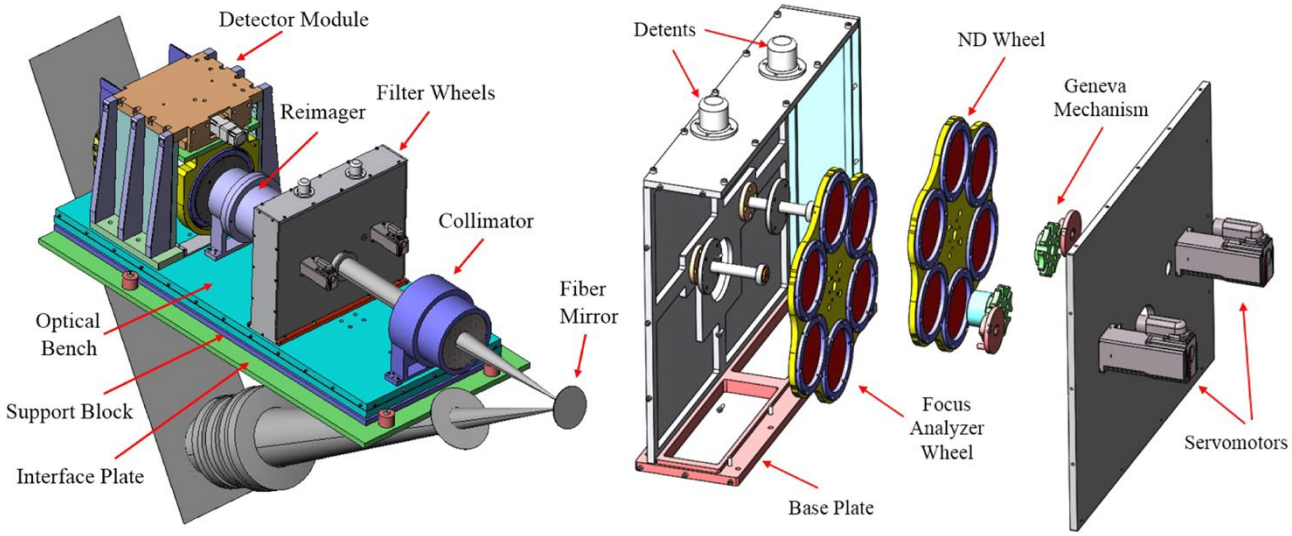

Figure 12: *Right Panel* – Mechanical design of the G-CLEF flexure control camera, *Left Panel* – Design of the focus analyzer/filter wheel system.

The issue of wavelength calibration is much less settled. For years, hollow cathode lamps with metallic thorium cathode were the standard calibrators for visible–band, high dispersion astronomical spectroscopy. Laser frequency combs (LFCs) have superb frequency stability (up to 1:10^{15}) and are extremely promising wavelength calibrators at the ~1 – 10 cm/sec precision level[13][14][12]. The virtues of lasers in general and LFCs in particular when compared to thorium light source has been discussed extensively in the literature[31][32]. A decade ago, the expectation was that LFCs would "automatically" replace thorium lamps.

The situation with respect to thorium cathode lamps has deteriorated, as there is no longer a commercial source for metallic thorium cathode lamps. Hollow cathode lamp manufacturers only offer thorium oxide cathodes, which perform poorly as wavelength calibrators[33]. Several LFCs are now commercially available with deployment costs in the $400k to $1M+ range, different SED passbands and various mean–time–between–failure (MTBF). Despite the anticipated precision of LFC calibration, 11 years of effort by instrumentation teams has failed to deliver on the promise of few cm/sec radial velocity precision in observation of stars or the Sun. It is to be emphasized that the internal accuracy of astronomical

velocimeters with LFCS has been demonstrated at the few cm/sec. This situation may be due to several factors, including the reluctance of observers to cede precious time on the world's most precise velocimeters to "engineering and experimentation". Recently, a generation of less expensive, more reliable LFCs has become available which have been benchmarked against heritage LFC systems at the HARPS-North facility, and the results of those experiments are promising[34]. Several groups have observational programs underway to refine wavelength scale calibration procedures and data reduction technique by observing the Sun with LFC–calibrated PRV instruments, however these investigations are still underway and results are only of a preliminary nature[35][36].

An alternative strategy for ultraprecise wavelength scale calibration employs ultrastabilized etalons. These fall into two categories – passively stabilized etalons and actively stabilized etalon. Passively stabilized etalons are constructed of the lowest CTE material obtainable and residual CTE is compensated with slightly higher CTE materials[15][16]. Their temperature is highly stabilized during calibration operations. Actively stabilized etalons servo the etalon gap by locking to an extremely stable atomic frequency standard[17][18]. Etalons have the potential to extend the calibration range of LFC into the deep blue end of the spectrum, where LFCs work poorly or not at all. As in the case of LFCs, there is potential to vastly improve radial velocity measurement precision, however the direct evidence in observations of stars from ground based observatories that etalons enable more precise radial velocity measurements is lacking today.

The cost of LFCs is dropping and reliability is improving. However, it seems probable that etalons will always be less expensive than LFCs and considerably more reliable. The unavailability of metallic anode thorium lamps will certainly drive G-CLEF to adopt one of the three technologies that are in development to replace and improve on thorium lamps. It remains to be seen whether the cost, complexity and fragility of LFCs offers a performance advantage over one of the etalon technologies.

6. SCHEDULE AND STATUS

As of this writing, two major capital procurements have been made – the camera lens blanks and the echelle gratings. Both orders have been delivered (see Figure 13). The critical design review is scheduled for September 2018. At that time, non-recurring engineer activities for the composite optical bench will be complete.

The overall schedule for the GMT and first light instrumentation is presented in Fanson et al., these proceedings[1].

7. ACKNOWLEDGEMENTS

This work has been supported by the GMTO Corporation, a non-profit organization operated on behalf of an international consortium of universities and institutions: Arizona State University, Astronomy Australia Ltd, the Australian National University, the Carnegie Institution for Science, Harvard University, the Korea Astronomy and Space Science Institute, the São Paulo Research Foundation, the Smithsonian Institution, the University of Texas at Austin, Texas A&M University, the University of Arizona, and the University of Chicago.

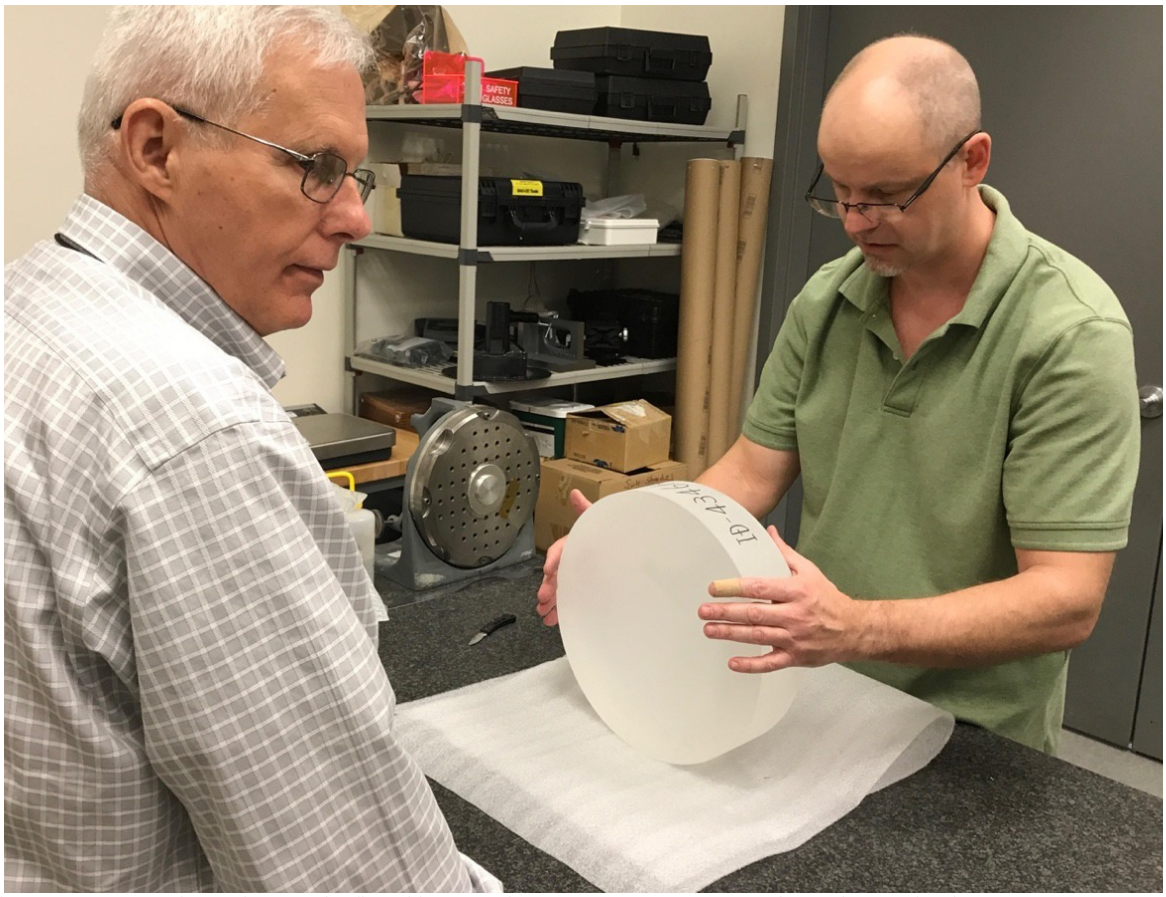

Figure 13: SAO engineers inspect the first shipment of a PBL25Y, 317 × 80 mm glass substrate for the G-CLEF cameras, delivered 2 May 2018.

REFERENCES

[1] Fanson, J., et al., "Overview and status of the Giant Magellan telescope project," Proc. SPIE 10700, 10700-34 (2018).
[2] Szentgyorgyi, A., et al., "The GMT-Consortium Large Earth Finder (G-CLEF): An optical echelle spectrograph for the Giant Magellan Telescope (GMT)", Proc. SPIE 9908, 990822 (2016).
[3] Szentgyorgyi, A., et al., "A preliminary design for the GMT-Consortium Large Earth Finder (G-CLEF)," Proc. SPIE 9147, 914726 (2014).
[4] Szentgyorgyi, A., et al., "The GMT-CfA, Carnegie, Catolica, Chicago Large Earth Finder (G-CLEF): a general purpose optical echelle spectrograph for the GMT with precision radial velocity capability," Proc. SPIE 8446, 84461H (2012).
[5] Mueller, M. et al., "Precision thermal control of the GMT-consortium large earth finder," Proc. SPIE 10702, 10702-368 (2018).
[6] Mueller, .M et al., "The opto-mechanical design of the GMT-consortium large Earth finder (G-CLEF)," SPIE 10702, 10702-359 (2018).
[7] Ben-Ami, S., et al., "New features in the optical design of the GMT-consortium large Earth finder," Proc. SPIE 10702, 10702-349 (2018).
[8] Ben-Ami S., et al., "The optical design of the G-CLEF Spectrograph: the first light instrument for the GMT," *Proc. SPIE* 9908, Ground-based and Airborne Instrumentation for Astronomy VI (2016).
[9] Oh, J., et al., "Detailed design of the G-CLEF flexure control camera subsystem," Proc. SPIE 10702, 10702-326 (2018).

[10] Evans, I.N., et al., "The preliminary design of the G-CLEF spectrograph instrument device control system," Proc. SPIE 10707, 10707-50 (2018).
[11] Pepe, F., Lovis, C., Segransen, D., Benz, W., Bouchy, F., Dumusque, X., Mayor, M., Queloz, D., Santos, N and Udry, S., "The HARPS search for Earth–like planets in the habitable zone. I. Very low-mass planets around HD20794, HD85512 and HD192310," A&A, 534, 58–74 2011).
[12] Li, C–H, et al.," A laser frequency comb that enables radial velocity measurements with a precision of 1 cms^{-1}," Nature, 452, 610–662 (2008).
[13] Murphy, M., et al.," High-precision wavelength calibration with laser frequency combs," MNRAS, 380, 839-847 (2007).
[14] Araujo–Hauck, C., et al., "Future wavelength calibration standards at ESO: the laser frequency comb," ESO Messenger, 129, 24-26 (2007).
[15] Wildi, F., Pepe, F., Chazelas, B., LoCurto, G. and Lovis, C., "The performance of the new Fabry-Perot calibration system of the radial velocity spectrograph HARPS," Proc. SPIE, 8151, 81511F (2011).
[16] Wildi, F., Chazelas, B. and Pepe, F., "A passive cost-effective solution for the high accuracy wavelength calibration of radial velocity spectrographs," Proc. SPIE, 8446, 84468E (2012).
[17] Sturmer, J., Seifahrt, A., Schwab, C. and Bean, J., "Rubidium-traced white-light etalon calibrator for radial velocity measurements at the cm s-1 level," JATIS, 3, 025003 (2017).
[18] McCracken, T., Jurgenson, C., Fischer, D., Stoll, R., Szymkowiak, A., Bradford, J. and Rutter, W., " Single-lock: a stable Fabry-Perot based wavelength calibrator," 91478, 91473L (2014).
[19] Ricker, G., et al, "Transiting Exoplanet Survey Satellite (TESS)," JATIS, 1, 014003 (2015).
[20] Rodler, F. and Lopez-Morales, M., "Feasibility Studies for the Detection of O2 in an Earth-like Exoplanet," ApJ, 781, 54 (2014).
[21] Snellen, I., de Kok, R., le Poole, R., Brogi, M and Birkby, J., " Finding Extraterrestrial Life Using Ground-based High-dispersion Spectroscopy,", ApJ, 764, 182 (2013).
[22] Kasen, D., Metzger, B., Barnes, J., Quataert, E. & Ramirez-Ruiz, E., "Origin of the Heavy Elements in Binary Neutron-Star Mergers from a Gravitational-Wave Event," Nature, 551, 80 (2017).
[23] Ji, A., Frebel, A., Simon, J. and Chiti, A.," Complete Element Abundances of Nine Stars in the r-process Galaxy Reticulum II," ApJ, 830, 93 (2016).
[24] Frebel, A., Christlieb, N., Norris, J., Thom, C., Beers, T. & Rhee, J, "Discovery of HE 1523-0901, a Strongly r-Process-enhanced Metal-poor Star with Detected Uranium," ApJ, 660, 117 (2007).
[25] Lawrence, J., et al., "Wide-field multi-object spectroscopy with MANIFEST," SPIE 10700, 10702-372 (2018).
[26] Jaffe, D., Barnes, S., Brooks, C., Lee, H., Mace, G., Pak, S., Park, B.–G. and Park, C., "GMTNIRS:progress toward the Giant Magellan Telescope near-infrared spectrograph," Proc. SPIE, 9908, 990821 (2016).
[27] Furesz, G., et al. "The G-CLEF spectrograph optical design," Proc. SPIE, 9147, 91479G (2014).
[28] Mueller, M., et al., "The opto-mechanical design of the GMT-Consortium Large Earth Finder (G-CLEF)," Proc. SPIE, 9908, 9908A2 (2016).
[29] Podgorski, W., et al., "A novel systems engineering approach to the design of a precision radial velocity spectrograph: the GMT-Consortium Large Earth Finder (G-CLEF)," Proc.SPIE, 9147, 91478W (2014).
[30] McLeod, B., et al.," The acquisition, guiding, and wavefront sensing system for the Giant Magellan telescope," Proc. SPIE, These proceedings, 10700-80 (2018).
[31] Szentgyorgyi, A., et al.," Deploying comb and tunable lasers to enable precision radial velocity surveys," Proc SPIE, 7014, 70141W (2008).
[32] LoCurto, et al., "Astronomical Spectrograph Calibration at the Exo-Earth Detection Limit," ESO Messenger, 149, 2–6, 2012.
[33] Fischer, D. et al., "State of the Field: Extreme Precision Radial Velocities," PASP, 128, 066001 2016.
[34] Ravi, A., et al., "Astro-comb calibrator and spectrograph characterization using a turn-key laser frequency comb," JATIS, 3, 045003 (2017).
[35] Dumusque, X., et al., "HARPS-N Observes the Sun as a Star," ApJL, 814, L21 (2015).
[36] Phillips, D., et al., " An astro-comb calibrated solar telescope to search for the radial velocity signature of Venus," Proc. SPIE, 9912, 99126Z (2016)